Probing dark matter in the Madala model using radio observations

R K Temo[1] and G M Beck

School of Physics and Centre for Astrophysics, University of the Witwatersrand, Johannesburg, Wits 2050, South Africa

E-mail: temokhilly@gmail.com

Abstract. The Madala (or 2HDM+S) model was introduced to explain several anomalies observed at the Large-Hardon-Collider. This model introduces an extra Higgs doublet (2HDM) and an additional scalar boson S. Furthermore, a dark matter candidate can be accomodated, coupling to the standard model via the S boson. Using the 2HDM+S dark matter parameter space previously found to fit the AMS-02 cosmic ray, and Fermi-LAT gamma-ray excesses we make synchrotron emission predictions and compare it with radio observations in variety of targets. The regions of interest for the predictions are M31 (or Andromeda galaxy) as well as the Coma and Ophiuchus galaxy clusters. The 3σ exclusion limits produced in this work do not exclude the Madala model that best fits the cosmic-ray and gamma-ray excesses.

1. Introduction

Madala model extends the Higgs-sector of the standard model (SM) by introducing bosons heavier than the SM Higgs boson h. The bosons introduced are the Madala boson H and a Higgs-like scalar mediator S. Parameters of the model are fixed such that $m_H = 270\ GeV$, $m_S = 150\ GeV$ and assuming the dominance of the decay mode $H \to Sh, SS$ [1]. In essence the model was postulated to explain the anomalous features seen in Run-1 [1, 2] and Run-2 data [3] at the LHC. The particular anomalies include the Higgs boson's transverse momentum p_T and the event excesses in the multi-leptons final states [1, 2, 4, 5, 6]. Interestingly, the model also provides a dark matter (DM) candidate χ. In this work, we try to constrain χ from an astrophysical standpoint.

The regime for using radio-band for indirect DM search was prominently advocated in Ref. [7], and the field has been active ever since. For example, Ref. [8] performed a radio-frequency indirect DM search using the Australian Compact Telescope Array (ATCA) instrument, and highly competitive constraints were placed on the DM annihilation cross-section of DM particles (model-independent). However, in this work, we employ a model-dependent approach for the indirect DM searches.

In this work we extend the previous work in [9], where χ was constrained using the cosmic-ray (positrons and anti-protons) excesses observed by the Alpha Magnetic Spectrometer (AMS-02) [10, 11] and the excesses seen by Fermi-LAT [12] in gamma-ray fluxes from the Milky-Way's galactic centre. The parameter space that best fits the aforementioned excesses is employed to make radio emission predictions for the sources, M31, Coma cluster and Ophiuchus cluster. The predicted DM synchrotron fluxes, from the 2HDM+S model, are compared to radio data in M31

as well as the Coma and Ophiuchus galaxy clusters to produce the 3σ level exclusion limit. We find that the radio data for the sources considered in this work do not exclude the 2HDM+S model. This is the case when both Einasto and NFW halo are considered for the 2HDM+S parameter space. It is worth highlighting that M31 place more robust limits as compared to the Coma and Ophiuchus cluster.
This paper is structured as follows; Section 2 describes the synchrotron emission from DM annihilations. Section 3 discusses the DM halos environment that governs our DM targets. Finally in Section 4 results are depicted and discussed.

2. Synchrotron Emission from Dark Matter Annihilation

Since the regime of interest is the radio band, we consider the synchrotron emission from the DM annihilation induced positrons. We consider the DM annihilation through S according to $2 \to 2$ scattering. The cascade of the scattering process follows $\chi\overline{\chi} \to S \to x$ (where x corresponds to some SM product). The source function for the SM products i (positrons or electrons) with energy E is given by,

$$Q_i(E, \vec{x}) = \frac{1}{2}\langle\sigma V\rangle_f \sum_f \frac{dN_i^f}{dE} B_f \left(\frac{\rho_\chi}{M_\chi}\right)^2 , \tag{1}$$

where $\langle\sigma V\rangle$ denotes the thermally velocity-averaged DM annihilation cross-section at 0 K,f denotes the kinematically allowed annihilation states with the branching ratio B_f, dN_i^f/dE denotes the production spectra for the SM products taken from the 2HDM+S model [9], the factor $(\rho/M_\chi)^2$ (where M_χ, ρ_χ denote the dark matter mass and density respectively) yields the dark matter pair density at the given position $\vec{x}$ within the galactic halo. The average power per positron with energy E is given by [13],

$$P_{\rm synch}(\nu, E, r, z) = \int_0^\pi \frac{\sin^2\theta}{2} 2\pi\sqrt{3} r_e m_e c \nu_g F_{\rm synch}\left(\frac{\kappa}{\sin\theta}\right) d\theta , \tag{2}$$

where ν denotes the observed frequency, r denotes the position within the halo, z denotes the redshift of the source of interest, r_e denotes the electron's classical radius, m_e denotes the electron's mass, c is the speed of light in vacuum, and finally, ν_g denotes the gyro-frequency for the non-relativistic case. Then the parameters κ and F_{synch} are further defined by,

$$\kappa = \frac{2\nu(1+z)}{3\nu_g\gamma^2}\left(1 + \left(\frac{\gamma\nu_p}{\nu(1+z)}\right)^2\right)^{\frac{3}{2}} , \tag{3}$$

with the ν_p denoting the plasma frequency which turns out to be directly proportional to $\sqrt{n_e}$, and γ denotes the Lorentz factor of the positron. Additionally, the synchrotron kernel is given by,

$$F_{\rm synch}(x) = x\int_x^\infty K_{5/3}(y)dy \approx 1.25 x^{\frac{1}{3}} e^{-x}\left(648 + x^2\right)^{\frac{1}{12}} . \tag{4}$$

Then the emissitivity of synchrotron radiation is given by,

$$j_{\rm synch}(\nu, r, z) = \int_{m_e}^{M_\chi}\left(\frac{dn_{e^-}}{dE} + \frac{dn_{e^+}}{dE}\right) P_{\rm synch}(\nu, E, r, z) dE , \tag{5}$$

where dn_{e^+}/dE and dn_{e^-}/dE are positron and electron equilibrium distributions respectively (see below for their explanation). By integrating over the volume of interest then we have the

flux density spectrum within the halo radius r given by,

$$S_{\rm synch}(\nu, z) = \int_0^r \frac{j_{\rm synch}(\nu, r^{'}, z)}{4\pi \left(D_L^2 + \left(r^{'}\right)^2\right)} d^3 r^{'} \ , \tag{6}$$

where the D_L denotes the luminosity distance to the DM halo of interest.
To account for diffusion and energy loss by electrons/positrons from DM annihilation, for an assumption where the processes of reacceleration and convection are negligible, the diffusion-loss equation is given by,

$$\frac{\partial}{\partial t}\frac{dn_e}{dE} = \nabla\left(D(E, \mathbf{x})\nabla\frac{dn_e}{dE}\right) + \frac{\partial}{\partial E}\left(b(E, \mathbf{x})\frac{dn_e}{dE}\right) + Q_e(E, \mathbf{x}) \ , \tag{7}$$

where $D(E, \mathbf{x})$ denotes the spatial diffusion function and $b(E, \mathbf{x})$ denotes the energy loss rate. A fully detailed analysis of the solutions to equation (7) can be found in [14]. The spatial diffusion is given by [14],

$$D(E) = D_0 \left(\frac{d_0}{1{\rm kpc}}\right)^{\frac{2}{3}} \left(\frac{\bar{B}}{1\mu G}\right)^{-\frac{1}{3}} \left(\frac{E}{\rm GeV}\right)^{\frac{1}{3}} \ , \tag{8}$$

where the diffusion constant $D_0 = 3.1 \times 10^{28}$ cm^{2}s^{-1}, $\bar{B}$ denotes the average magnetic field and d_0 denotes the smallest scale where the magnetic field is found to be homogenous. The energy loss rate is given by [7],

$$b(E) = b_{\rm IC}E^2\left[1+z\right]^4 + b_{\rm synch}E^2\bar{B}^2 + b_{\rm coul}\bar{n}\left[1 + \frac{1}{75}\log\left(\frac{\gamma}{\bar{n}}\right)\right] + b_{\rm brem}\bar{n}\left[\log\left(\frac{\gamma}{\bar{n}}\right) + 0.36\right] \ , \tag{9}$$

where $\bar{n}$ denotes the average electron density, $\gamma = E/m_e c^2$ denotes the electron Lorentz factor, while $b_{\rm IC}$, $b_{\rm synch}$, $b_{\rm Coul}$ and $b_{\rm brem}$ are inverse-Compton, synchrotron, Coulomb and bremsstrahlung energy loss factor. These take values 0.25, 0.0254, 6.13 and 1.51 in units 10^{-16} GeVs^{-1} respectively.

3. Dark Matter Halos Environment

In this section we discuss the halo environments that characterise M31, Coma and Ophiuchus. More attention is given to the magnetic field and thermal electron density distribution for sources under consideration.

3.1. M31

For M31 we assume the halo data from [15] at a distance 770 kpc. For the virial mass of $1.04 \times 10^{12} M_\odot$ the halo density profile is given by Navarro-Frenk-White (NFW) profile [16],

$$\rho_{\rm NFW}(r) = \frac{\rho_s}{\frac{r}{r_s}\left(1 + \frac{r}{r_s}\right)^2} \ , \tag{10}$$

where ρ_s denotes the characteristic density and r_s denotes the scale radius. For the magnetic field profile we follow [17],

$$B(r) = \frac{4.6 r_1 + 64}{r_1 + r}\mu G \ , \tag{11}$$

where $r_1 = 200$ kpc as suggested by fittings in [17]. For $r = 14$ kpc the magnetic field strength is taken to be $B = 4.6 \pm 1.2\ \mu G$. The thermal electron density distribution follows an exponetial profile from [17],

$$n_e(r) = n_0 \exp\left(-\frac{r}{r_d}\right) \ , \tag{12}$$

where central density is taken to be $n_0 = 0.06$ cm^{-3} and r_d is the disk scale radius which is approximately 5 kpc [17]. We predict synchrotron emission fluxes for frequencies between $50 - 10^9$ MHz for M31. Subsequently, this is compared to the low frequency 408 MHz point flux [18] for a rather optimistic region of interest (50 arcminutes).

3.2. Coma Cluster

For the Coma cluster the virial mass is $1.33 \times 10^{15} M_\odot$ and virial concentration $c_{\rm vir} = 10$, at the redshift $z = 0.0231$. Similar to M31 we use NFW density profile for Coma. For the thermal electron density distribution in Coma we follow [19, 20],

$$n_e(r) = n_0 \left(1 + \left[\frac{r}{r_s}\right]^2\right)^{-q_e} , \tag{13}$$

where $n_0 = 3.49 \times 10^{-3}$ cm^{-3} and $q_e = 0.981$. The magnetic field profile in Coma is given by [21],

$$B(r) = B_0 \left(\frac{n_e(r)}{n_0}\right)^{q_b} , \tag{14}$$

where $B_0 = 4.7$ μG and $q_b = 0.5$. The fittings from [21] suggest a magnetic field with a Kolmogorov power spectrum characterised by a minimal coherence length $\Lambda_{min} \approx 2$ kpc. We predict $50 - 10^9$ MHz synchrotron emission fluxes for Coma. For a region of interest of about 30 arcminutes, the Coma radio fluxes data from [22] with a frequency range $30.9 - 4850$ MHz was compared with the predicted radio fluxes.

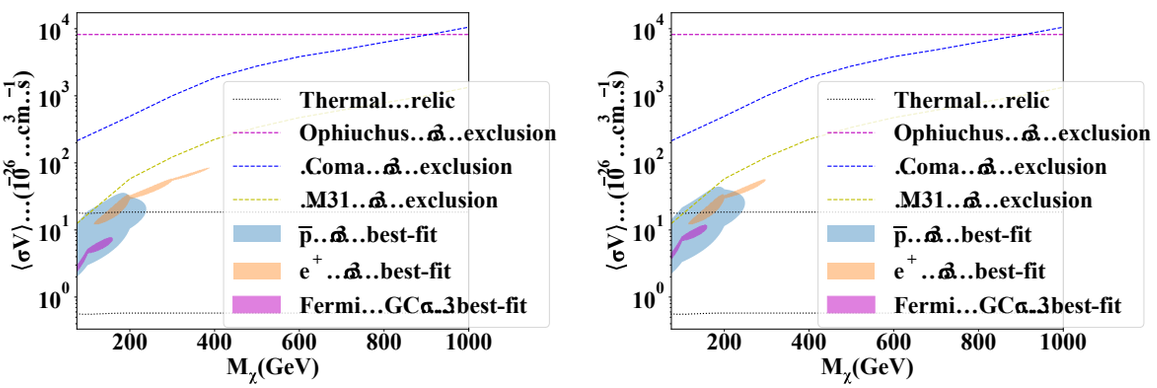

Figure 1. Depicts $2 \to 2$ best-fit parameter space to the AMS-02 positron, anti-proton spectra and Fermi-LAT galactic excesses. The contours are 3σ confidence intervals on the M_χ and $\langle \sigma V \rangle$ plane. The thermal relic [23] is denoted as a band to account for uncertainties in the local DM density and halo profile. Dashed lines denote 3σ exclusion limits for M31 (yellow), Coma (blue) and Ophiuchus (Magenta). Left: For Einasto halo profile. Right: For NFW halo profile.

3.3. Ophiuchus Cluster

For the Ophiuchus cluster we assume halo data from [24]. The virial mass is $1.1 \times 10^{15} M_\odot$ and virial radius is given by $r_{vir} = 2.1$ Mpc at the redshift $z = 0.0296$. Even here we will employ the NFW density profile. In terms of the magnetic field and the thermal electron density distribution we adhere to the formalism in [25] which assumes that Ophiuchus follows profiles similar to that in Coma, where $B_0 = 5.225$ μG, $q_b = 0.74$, $n_0 = 0.29614$ and $q_e = 0.412725$.

 ISBN: 978-0-620-97693-0

Even here, we predict $50 - 10^9$ MHz synchrotron emission fluxes for Ophiuchus. Subsequently, this is compared to the 153, 240 and 1477 MHz, radio fluxes from [26] for a region of interest of about 7 arcminutes.

4. Results and Discussion

We make use of the parameter space that best-fits the cosmic-ray and gamma-ray excesses produced in [9] for both NFW and Einasto halos. This parameter space gives annihilating DM through the Madala model to induce highly energetic positrons, which in the presence of a magnetic field emits synchrotron emission in M31, Coma and Ophiuchus. Following the recipe delineated in both Section 2 and 3, synchrotron emission predictions were made. Comparing the predicted synchrotron emission fluxes with M31 [18], Coma [22] and Ophiuchus [26] radio observation data, 3σ exclusion limits were produced to match our previous work parameter space. The M31 radio data used here have been highly constraining in other DM models (see e.g [27]). In figure 1, we observe that M31 has better constraining limits transcending those of Coma and Ophiuchus. Significantly, all the exclusion limits do not exclude our Madala DM model. With the radio DM-search regime entering a new era of high sensitivity and resolution, this will aid to place more stringent limits on the Madala model in near future. MeerKAT is one of the exciting detectors that may be able to probe the DM interpretation offered by the Madala model as elucidated in [9]. More interestingly, the full-SKA has the potential of probing the parameter space of the Madala model at 5σ confidence level within 100 hours observation time [9].

Acknowledgments

We acknowledge Elias Malwa, Mukesh Kumar and Bruce Mellado for useful insights regarding the Madala model. This work was supported by South African National Research Foundation, and the South African Research Chair Initiative of the Department of Science and Technology and National Research Foundation. GB acknowledges the funding of the National Research Foundation through Thuthuka grant number 117969.

References

[1] Von Buddenbrock S, Chakrabarty N, Cornell A S, Kar D, Kumar M, Mandal T, Mellado B, Mukhopadhyaya B, Reed R G and Ruan X 2016 *Eur. Phys. J. C* **76** 1–18
[2] Von Buddenbrock S, Chakrabarty N, Cornell A S, Kar D, Kumar M, Mandal T, Mellado B, Mukhopadhyaya B and Reed R G 2015 The compatibility of LHC run 1 data with a heavy scalar of mass around 270 GeV *Preprint* hep-ph/1506.00612
[3] Von Buddenbrock S, Cornell A S, Mohammed A F, Kumar M, Mellado B and Ruan X 2018 *J. Phys. G Nucl. Part. Phys.* **45** 115003
[4] Kumar M, von Buddenbrook S, Chakrabarty N, Cornell A S, Kar D, Mandal T, Mellado B, Mukhopadhyaya B and Reed R G 2017 The impact of additional scalar bosons at the LHC *Journal of Physics: Conf. Series* vol 802 (IOP Publishing) p 012007
[5] von Buddenbrock S, Cornell A S, Kumar M and Mellado B 2017 The Madala hypothesis with run 1 and 2 data at the LHC *Journal of Physics: Conf. Series* vol 889 (IOP Publishing) p 012020
[6] von Buddenbrock S 2017 Exploring LHC run 1 and 2 data using the Madala hypothesis *Journal of Physics: Conf. Series* vol 878 (IOP Publishing) p 012030
[7] Colafrancesco S, Profumo S and Ullio P 2007 *Phys. Rev. D* **75** 023513
[8] Regis M, Richter L and Colafrancesco S 2017 *J. Cosmol. Astropart. Phys.* **2017** 025
[9] Beck G, Temo R, Malwa E, Kumar M and Mellado B 2021 Connecting multi-lepton anomalies at the LHC and in astrophysics and the prospects of MeerKAT/SKA *Preprint* astro-ph.HE/2102.10596
[10] Aguilar M, Cavasonza L A, Ambrosi G, Arruda L, Attig N, Azzarello P, Bachlechner A, Barao F, Barrau A, Barrin L *et al.* 2019 *Phys. Rev. Lett.* **122** 041102
[11] Aguilar M, Cavasonza L A, Alpat B, Ambrosi G, Arruda L, Attig N, Aupetit S, Azzarello P, Bachlechner A, Barao F *et al.* 2016 *Phys. Rev. Lett.* **117** 091103

[12] Ackermann M, Ajello M, Albert A, Atwood W, Baldini L, Ballet J, Barbiellini G, Bastieri D, Bellazzini R, Bissaldi E *et al.* 2017 *Astrophys. J.* **840** 43
[13] Longair M S 2010 *High energy astrophysics* (Cambridge University Press)
[14] Colafrancesco S, Profumo S and Ullio P 2006 *Astron. Astrophys.* **455** 21–43
[15] Tamm A, Tempel E, Tenjes P, Tihhonova O and Tuvikene T 2012 *Astron. Astrophys.* **546** A4
[16] Navarro J F 1996 The structure of cold dark matter halos *Symp.-Int. astronomical union* vol 171 (Cambridge University Press) pp 255–258
[17] Ruiz-Granados B, Rubiño-Martín J, Florido E and Battaner E 2010 *Astrophys. J. Lett.* **723** L44
[18] Ficarra A, Grueff G and Tomassetti G 1985 *Astron. astrophys., Suppl. ser. (Print)* **59** 255–347
[19] Łokas E L and Mamon G A 2003 *Mon. Notices Royal Astron. Soc.* **343** 401–12
[20] Chen Y, Reiprich T, Böhringer H, Ikebe Y and Zhang Y Y 2007 *Astron. Astrophys.* **466** 805–12
[21] Bonafede A, Feretti L, Murgia M, Govoni F, Giovannini G, Dallacasa D, Dolag K and Taylor G 2010 *Astron. Astrophys.* **513** A30
[22] Thierbach M, Klein U and Wielebinski R 2003 *Astron. Astrophys.* **397** 53–61
[23] Steigman G, Dasgupta B and Beacom J F 2012 *Phys. Rev. D* **86** 023506
[24] Durret F, Wakamatsu K i, Nagayama T, Adami C and Biviano A 2015 *Astron. Astrophys.* **583** A124
[25] Beck G 2020 *Mon. Notices Royal Astron. Soc.* **494** 1128–32
[26] Murgia M, Eckert D, Govoni F, Ferrari C, Pandey-Pommier M, Nevalainen J and Paltani S 2010 Gmrt observations of the ophiuchus galaxy cluster *Preprint* astro-ph.CO/1002.2332
[27] Beck G 2019 *J. Cosmol. Astropart. Phys.* **2019** 019